Ari Laiho and Olli Ikkala. 2007. A rheo-optical apparatus for real time kinetic studies on shear-induced alignment of self-assembled soft matter with small sample volumes. Review of Scientific Instruments, volume 78, number 1, 015109.

The following article appeared in Review of Scientific Instruments, volume 78, number 1, 015109, and may be found at
http://link.aip.org/link/?rsi/78/015109

A rheo-optical apparatus for real time kinetic studies on shear-induced alignment of self-assembled soft matter with small sample volumes

Ari Laiho[a] and Olli Ikkala
Department of Engineering Physics and Mathematics and Center for New Materials, Helsinki University of Technology, P.O. Box 2200, FI-02015 HUT, Espoo, Finland

(Received 24 March 2006; accepted 21 November 2006; published online 24 January 2007)

In soft materials, self-assembled nanoscale structures can allow new functionalities but a general problem is to align such local structures aiming at monodomain overall order. In order to achieve shear alignment in a controlled manner, a novel type of rheo-optical apparatus has here been developed that allows small sample volumes and *in situ* monitoring of the alignment process during the shear. Both the amplitude and orientation angles of low level linear birefringence and dichroism are measured while the sample is subjected to large amplitude oscillatory shear flow. The apparatus is based on a commercial rheometer where we have constructed a flow cell that consists of two quartz teeth. The lower tooth can be set in oscillatory motion whereas the upper one is connected to the force transducers of the rheometer. A custom made cylindrical oven allows the operation of the flow cell at elevated temperatures up to 200 °C. Only a small sample volume is needed (from 9 to 25 mm^3), which makes the apparatus suitable especially for studying new materials which are usually obtainable only in small quantities. Using this apparatus the flow alignment kinetics of a lamellar polystyrene-*b*-polyisoprene diblock copolymer is studied during shear under two different conditions which lead to parallel and perpendicular alignment of the lamellae. The open device geometry allows even combined optical/x-ray *in situ* characterization of the alignment process by combining small-angle x-ray scattering using concepts shown by Polushkin *et al.* [Macromolecules **36**, 1421 (2003)]. © *2007 American Institute of Physics.* [DOI: 10.1063/1.2409870]

I. INTRODUCTION

Self-assembly allows nanoscale structures within soft matter due to competing interactions, based on, e.g., block copolymers, liquid crystals, amphiphiles, and their supramolecular combinations.[1–4] The length scale and morphology of the self-assembled order can be selected by the constituent moieties. For example, in block copolymers the morphologies can be systematically controlled by changing the number of structural units, their lengths, and their chemical compositions and diblock copolymers can self-assemble into, e.g., lamellae, hexagonally arranged cylinders or a cubic array of spheres. However, self-assembly typically leads to polydomain structures consisting of locally anisotropic ordered domains but their random orientation leads to macroscopically isotropic materials. Concerning potential applications this macroscopic isotropy is not often wanted and external fields such as electric, magnetic, or flow fields are used to extend the nanoscale structures into the macroscale and thus to obtain favorable anisotropic properties.[5–8] Large amplitude oscillatory shear flow (LAOS) has proved to be an exceptionally feasible method to extend the locally self-assembled nanostructures of molten block copolymers in particular into macroscopically aligned state.[5,6,9–12] The ultimate aligned state of the material depends on four different parameters, namely, the oscillation frequency, shear strain amplitude, duration of shear, and temperature. Because the structure characterization of the aligned material is usually performed *ex situ* using, e.g., transmission electron microscopy (TEM) or small-angle scattering of either x-rays or neutrons (SAXS or SANS), conducting a series of routine experiments can be really time consuming and the feasible processing parameters cannot be identified. Hence a need for an *in situ* method that can give information on the evolution of the structure already during the shear alignment arises. Both *in situ* SAXS[13,14] and SANS[15,16] methods have been reported in literature. The scattering experiments require high intensity beam in order to obtain reasonable time resolution. For instance synchrotron radiation typically must be employed for *in situ* SAXS measurements in order to obtain high enough brilliance and thus performing a series of preliminary screening measurements is most often not an option.

Flow birefringence which is sensitive to the degree of alignment has also been used widely to probe the microstructural evolution during shear.[5] It has been shown to be a feasible method to follow the fast alignment processes in general as time resolution can be as low as 10 ms. Combining the method with *ex situ* characterization techniques, such as SAXS and TEM has proved to be exceptionally powerful.[17] Flow birefringence of a block copolymer can be divided into two distinct contributions: intrinsic (Δn_i) and form birefringence (Δn_f). The former originates from the anisotropy in the polymer monomer and is proportional to the stress in the polymer chain whereas the latter is related to a

[a]Author to whom correspondence should be addressed; electronic mail: ari.laiho@hut.fi

much larger length scale and results from the block copolymer microstructure. Birefringence has been used successfully for real-time kinetic studies on shear aligning diblock copolymers both for systems where the self-assembled domains have significantly different[9] ($\Delta n_f \gg \Delta n_i$) and nearly equal[18] ($\Delta n_i \gg \Delta n_f$) refractive indices.

The aim of the present work is to develop a new rheo-optical apparatus for studying shear alignment kinetics of polymer melts. The emphasis of the design was focused on an innovative measurement geometry allowing small sample volumes, easy removal of the sample, and easy access for both the optic beam and an optional x-ray beam. These characteristics are not found in any other rheo-optic apparatus reported in the literature or commercially available device. As a comparison the typical geometry for the optical analysis module (TA Instruments, New Castle, DE) is made of two polished quartz plates of 40 mm in diameter. This geometry requires a sample volume of 1250 mm^3 for a 1 mm thick sample whereas the measurement geometry described in the present work requires only 9–25 mm^3 for a 1 mm thick sample depending on the chosen tooth size. The measurement setup introduced by Kornfield and co-workers[5] offers smaller sample volumes than the commercial alternative but sample removal and replacement of the windows is more difficult than in our setup and in addition the geometry cannot offer as easy access for another beam (e.g., an x-ray beam) in orthogonal direction with respect to the optical beam.

II. DESIGN OF THE APPARATUS

A. General design considerations

In general, for new materials the obtainable sample quantities are usually small and thus one must use as small sample geometries as possible in the rheo-optical studies. Decreasing the size of the flow cell, however, increases the error in the rheological parameters and thus a compromise must be made between the size of the sample geometry and the accuracy of the rheological measurements. Our motivation is more focused upon inducing shear alignment on new materials than on thorough rheological characterization and thus the passage toward smaller geometry is natural. But then again, Polushkin *et al.* have shown that despite the small sample geometry and considerable gap/width ratio adequate rheological measurement can still be performed.[14,19]

An overall scheme of the rheo-optical setup is shown in Fig. 1. Construction of a special device to impose shear flow was not needed as a rheometer is a suitable platform for that purpose. A commercial Bohlin VOR shear strain controlled rheometer (Bohlin Reologi AB) was chosen because it can offer enough space for implementing the optical setup and an oven.

B. Rheometer and flow cell

The flow cell consists of two rectangular fused silica (Suprasil quartz) teeth between which the sample is placed (see Fig. 2). The teeth offer a cheap alternative to parallel quartz plates and in addition they can be easily removed and replaced. Fused silica was chosen for the material both for its

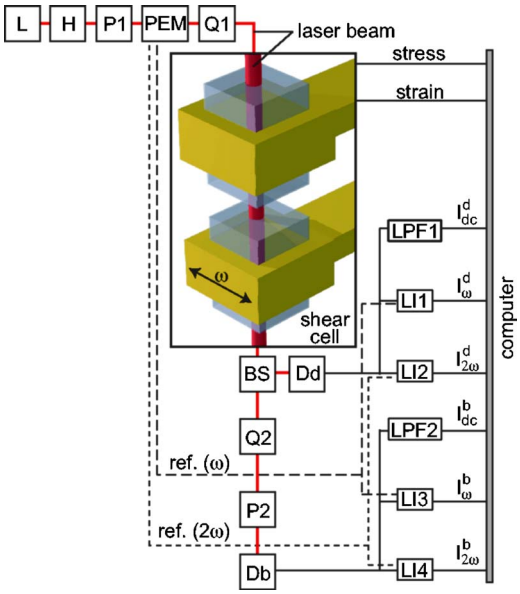

FIG. 1. (Color online) Schematic illustration of the apparatus: (L) laser; (H) half-wave plate; (P) polarizer; (PEM) photoelastic modulator; (Q) quarter-wave plate; sample in the shear cell; (BS) beam splitter; (Dd) detector for dichroism path; (Db) detector for birefringence path; (LPF) low-pass filter; (LI) lock-in amplifier.

thermal and mechanical properties as well as because the teeth must be made of an isotropic material that does not change the polarization state of the incoming light beam and is highly transparent to the wavelength being used. The teeth are attached to brass shafts the lower of which is connected to the rheometer motor and can be subjected to oscillatory motion whereas the upper shaft is connected to the torque and normal force transducers of the rheometer. The sample is then placed between the two quartz teeth while the thickness of the sample and thus the path length of the optical beam can be monitored with a thickness meter (Mitutoyo, IDC-112B). The lower tooth is now put in sinusoidal motion and the upper tooth senses the shear stress subjected to the sample meanwhile the laser beam may travel through the teeth and the sample 25 mm away from the rotation axis. The design of the shafts allows use of different sized teeth, namely, 3×3, 3×5, 4×4, and 5×5 mm^2 in cross section. Because the rheometer measures torque and angular velocity, conversion constants must be used to relate these variables to shear stress and shear rate respectively:

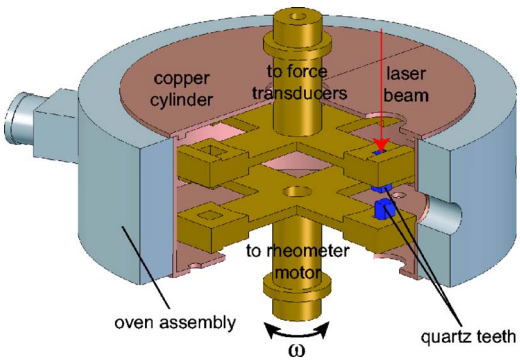

FIG. 2. (Color online) Schematic illustration of the flow cell and oven assembly.

$$\dot{\gamma} = C_2\Omega = \frac{R}{h}\Omega, \tag{1}$$

where $\dot{\gamma}$ is the shear strain rate, $R=25$ mm is the distance from the rotation axis to the center of each teeth, h is the thickness of the sample, and Ω is the angular velocity of the tooth. For the relation between torque (τ) and shear stress (σ) we get

$$\frac{\tau}{\sigma} = C_1^{-1} = \int_S dA = \int_{-a/2}^{a/2}\int_{R-(b/2)}^{R+(a/2)} \sqrt{x^2+y^2}\,dx\,dy, \tag{2}$$

where a and b are the width and depth of the tooth, respectively. The integral can be calculated in closed form but because the result is lengthy it is not shown here.

Custom made cylindrical heating element allows rheo-optic measurements at elevated temperatures up to 200 °C. The oven assembly is equipped with two different thermo-elements one placed directly to a copper cylinder surrounding the shafts and the other next to the upper tooth. The upper and lower covers of the oven have quartz windows. Two additional windows in the oven cylinder allow a free tangential access to the sample for e.g., an x-ray beam.

C. Optical setup

Flow birefringence and dichroism as well as their orientation angles are measured using an optical train based on the early work of Fuller and co-workers.[20] All of the optical elements are assembled on high precision rotation mounts in order to ease the alignment procedure.

The monochromatic light source is a helium-neon laser (L, see Fig. 1). The moderately polarized light (polarization ratio 500:1) of the laser is first passed through a half-wave plate (H) whose orientation angle with respect to the following high quality Glan Taylor polarizer (P1) can be used to adjust the light intensity. After passing through the first polarizer (P1) a photoelastic modulator (PEM, Hinds Instruments, Hillsboro, OR, PEM-90 I/FS50) induces a sinusoidally varying phase shift between the fast and slow axis component of the incident linearly polarized light according to

$$\Delta = \Delta_0 \sin(\omega t), \tag{3}$$

where Δ_0 is the retardation amplitude and $\omega=50$ kHz represents the modulation frequency. Subsequently the modulated beam is passed through a quarter-wave plate (Q1) and guided through the quartz teeth between which the sample is placed. Next the transmitted beam is split by a nonpolarizing beam splitter (BS) into dichroism and birefringence beams and the intensity of the former is measured using a photodiode (D_d, Hinds Instruments DET-90, model 002) whereas the birefringence beam is directed through a quarter-wave plate (Q2) and a polarizer (P2) to the second photodiode (D_b).

D. Signal analysis

The theoretical analysis of the experiment can be accomplished using Mueller calculus.[21] In this formalism each optical component is described with a single Mueller matrix $\boldsymbol{M}\in\mathbb{R}^{4\times4}$ whose elements depend on the optical activity of the component caused by both linear and circular birefringence and dichroism as well as their orientation angles with respect to a reference direction which in this case is the direction of the flow field. Furthermore the polarization state of light can be described by a Stokes vector $\boldsymbol{S}\in\mathbb{R}^4$ whose first element represents the intensity of light. The Stokes vector received at the detector $\boldsymbol{S}_1$ after the light beam has passed through all the components, including the sample $(\boldsymbol{M}_S)$, is now calculated by multiplying the Mueller matrices with the Stokes vector that describes the initial polarization state of light $\boldsymbol{S}_0$

TABLE I. Orientation angles of the optical components with respect to the flow direction. See Fig. 1 for definitions of the symbols.

	L[a]	H	P1	PEM	Q1	Q2	P2
Angle (°)	0	θ[b]	0	45	0	45	90

[a]Orientation angle refers to the polarizer of the laser.
[b]The intensity of light can be adjusted by changing the orientation angle of the half-wave plate.

$$\boldsymbol{S}_1 = \boldsymbol{M}_{\mathrm{PSA}}\boldsymbol{M}_S\boldsymbol{M}_{\mathrm{PSG}}\boldsymbol{S}_0, \tag{4}$$

where $\boldsymbol{M}_{\mathrm{PSG}}$ is the Mueller matrix of the polarization state generator (PSG) and $\boldsymbol{M}_{\mathrm{PSA}}$ is the Mueller matrix of the polarization state analyzer (PSA), i.e., the product of the Mueller matrices prior to and after the sample, respectively. The intensity measured at the detector is now the first element of the Stokes vector $\boldsymbol{S}_1$. This can also be expressed by means of Stokes vectors

$$I = I_0\boldsymbol{S}_{\mathrm{PSA}}^T\boldsymbol{M}_S\boldsymbol{S}_{\mathrm{PSG}}. \tag{5}$$

The orientation angles of the optical components in our setup are shown in Table I. When the orientation angles of the setup are known, the Mueller matrices or the Stokes vectors of the corresponding optical elements can be calculated. For the polarization state generator the Stokes vector can be written

$$\begin{aligned}\boldsymbol{S}_{\mathrm{PSG}} &= \boldsymbol{M}_Q(0)\boldsymbol{M}_{\mathrm{PEM}}(45,\Delta)\boldsymbol{M}_P(0)\boldsymbol{M}_H(\theta)\boldsymbol{M}_P(0)\boldsymbol{I}_0 \\ &= \frac{I_0}{4}(1+\cos(4\theta))\begin{bmatrix}1\\ \cos\Delta\\ \sin\Delta\\ 0\end{bmatrix} = I_1\begin{bmatrix}1\\ \cos\Delta\\ \sin\Delta\\ 0\end{bmatrix},\end{aligned} \tag{6}$$

where $\boldsymbol{M}_X(\alpha)$ refers to the Mueller matrix of the optical component X with orientation angle α and $\boldsymbol{I}_0=[I_0\ 0\ 0\ 0]^T$. Stokes vectors of the polarization state analyzer for dichroism and birefringence branch, respectively, can be written

$$\boldsymbol{S}_{\mathrm{PSAb}} = \frac{1}{2}\begin{bmatrix}1\\ 0\\ 0\\ -1\end{bmatrix},\quad \boldsymbol{S}_{\mathrm{PSAd}} = \begin{bmatrix}1\\ 0\\ 0\\ 0\end{bmatrix}. \tag{7}$$

Mueller matrix of a sample that exhibits both linear and circular dichroism and birefringence in the limit of small anisotropies can be expressed as

$$\boldsymbol{M}_S = \begin{bmatrix} 1 & -\delta' \cos(2\theta'') & -\delta' \sin(2\theta'') & \delta_c'' \\ -\delta' \cos(2\theta'') & 1 & \delta_c' & -\delta' \sin(2\theta') \\ -\delta' \sin(2\theta'') & -\delta_c' & 1 & \delta' \cos(2\theta') \\ \delta_c'' & \delta' \sin(2\theta') & -\delta' \cos(2\theta') & 1 \end{bmatrix}, \tag{8}$$

where δ' and θ' refer to linear retardation and its orientation angle, δ'' and θ'' refer to linear extinction and its orientation angle, and δ_c' and δ_c'' refer to circular retardation and extinction, respectively.

Bessel functions of the first kind can be used to expand the $\sin(\Delta)$ and $\cos(\Delta)$ terms in Eq. (6) according to

$$\sin(\Delta) = \sum_{k=0}^{\infty} 2J_{2k+1}(\Delta_0)\sin[(2k+1)\omega t], \tag{9}$$

$$\cos(\Delta) = J_0(\Delta_0) + \sum_{k=1}^{\infty} 2J_{2k}(\Delta_0)\sin(2k\omega t). \tag{10}$$

Now terms up to the second harmonic frequency are taken from the Eqs. (9) and (10) and the obtained expressions are substituted into Eq. (6). The intensity measured at the detectors D_d and D_b can now be calculated as follows:

$$\begin{aligned} I_{D_d} &= I_0 \boldsymbol{S}_{\mathrm{PSA}_d}^T \boldsymbol{M}_S \boldsymbol{S}_{\mathrm{PSG}} = I_1[1 - \delta' J_0(\Delta_0)\cos(2\theta'') \\ &\quad - 2\delta' J_1(\Delta_0)\sin(2\theta'')\sin(\omega t) \\ &\quad - 2\delta' J_2(\Delta_0)\cos(2\theta'')\cos(2\omega t)] \\ &= I_1[I_{dc}^d + I_\omega^d \sin(\omega t) + I_{2\omega}^d \cos(2\omega t)], \end{aligned} \tag{11}$$

$$\begin{aligned} I_{D_b} &= I_0 \boldsymbol{S}_{\mathrm{PSA}_b}^T \boldsymbol{M}_S \boldsymbol{S}_{PSG} = \frac{I_1}{2}[1 - \delta_c'' - J_0(\Delta_0)[\delta'' \cos(2\theta'') \\ &\quad + \delta' \sin(2\theta')] - 2J_1(\Delta_0)[\delta'' \sin(2\theta'') \\ &\quad - \delta' \cos(2\theta')]\sin(\omega t) - 2J_2(\Delta_0)[\delta'' \cos(2\theta'') \\ &\quad + \delta' \sin(2\theta')]\cos(2\omega t)] \\ &= \frac{I_1}{2}[I_{dc}^b + I_\omega^b \sin(\omega t) + I_{2\omega}^b \cos(2\omega t)]. \end{aligned} \tag{12}$$

The retardation amplitude Δ_0 can be chosen so that the time-independent terms I_{dc}^d and I_{dc}^b in Eqs. (11) and (12) become independent of δ and θ that is $J_0(\Delta_0 = 2.405) = 0$. These dc terms can be measured by passing the signals from both detectors through conventional low pass filters. The first and second harmonics of the signals (I_ω and $I_{2\omega}$) can be determined using lock-in amplifiers that are referenced to the PEM's modulation frequency. The obtained signals are further normalized with dc-terms in order to minimize the variations in the light intensity due to e.g., fluctuations in the light source. For the normalized signals we get

$$R_\omega^d = \frac{I_\omega^d}{I_{dc}^d} = -2\delta' J_1(\Delta_0)\sin(2\theta''), \tag{13}$$

$$R_{2\omega}^d = \frac{I_{2\omega}^d}{I_{dc}^d} = -2\delta' J_2(\Delta_0)\cos(2\theta''), \tag{14}$$

$$R_\omega^b = \frac{I_\omega^b}{I_{dc}^b} = -2J_1(\Delta_0)[\delta'' \sin(2\theta'') - \delta' \cos(2\theta')], \tag{15}$$

$$R_{2\omega}^b = \frac{I_{2\omega}^b}{I_{dc}^b} = -2J_2(\Delta_0)[\delta'' \cos(2\theta'') + \delta' \sin(2\theta')]. \tag{16}$$

These ratios can be used to determine δ', δ'', θ', and θ'' as follows:

$$|\delta''| = \frac{1}{2}\sqrt{\left(\frac{K_\omega^d R_\omega^d}{J_1(\Delta_0)}\right)^2 + \left(\frac{K_{2\omega}^d R_{2\omega}^d}{J_2(\Delta_0)}\right)^2}, \tag{17}$$

$$\theta'' = \frac{1}{2}\arctan\left(\frac{K_\omega^d R_\omega^d J_2(\Delta_0)}{K_{2\omega}^d R_{2\omega}^d J_1(\Delta_0)}\right), \tag{18}$$

$$|\delta'| = \frac{1}{2}\sqrt{\left(\frac{K_\omega^b R_\omega^b - K_\omega^d R_\omega^d}{J_1(\Delta_0)}\right)^2 + \left(\frac{K_{2\omega}^b R_{2\omega}^b - K_{2\omega}^d R_{2\omega}^d}{J_2(\Delta_0)}\right)^2}, \tag{19}$$

$$\theta' = \frac{-1}{2}\arctan\left(\frac{(K_{2\omega}^b R_{2\omega}^b - K_{2\omega}^d R_{2\omega}^d)J_1(\Delta_0)}{(K_\omega^b R_\omega^b - K_\omega^d R_\omega^d)J_2(\Delta_0)}\right), \tag{20}$$

where K_ω^d, $K_{2\omega}^d$, K_ω^b, and $K_{2\omega}^b$ are instrumental constants that relate the measured root mean square voltages to the intensities.

Birefringence and dicroism are related to these parameters via the following two equations:

$$|\Delta n'| = \frac{\lambda|\delta'|}{2\pi d}, \tag{21}$$

$$|\Delta n''| = \frac{\lambda|\delta''|}{2\pi d}, \tag{22}$$

where $\lambda = 632.8$ mm is the wavelength of the laser and d is the sample thickness.

III. RHEO-OPTICAL STUDIES: SHEAR-INDUCED ORIENTATION

A. Materials

Preliminary experiments to test the performance of the rheo-optic apparatus were carried out on a poly(isoprene)-*b*-poly(styrene) diblock copolymer [PS-*b*-PI, Polymer Source Inc. (Canada), $M_n = 11.5$-*b*-10.5 kg/mol, $M_w/M_n = 1.04$]. Below order disorder transition temperature (T_ODT) the material microphase separates into a lamellar morphology with a period of $d = 216$ Å.

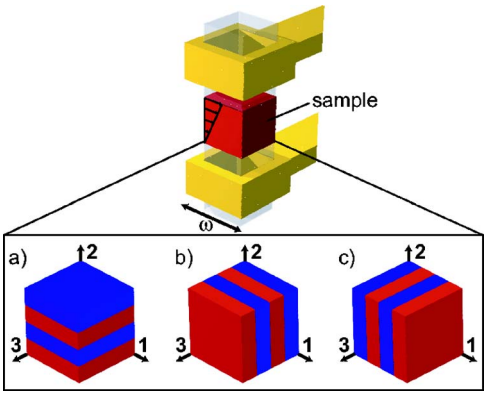

FIG. 3. (Color online) Schematic illustration of the possible macroscale shear-induced alignments for a sample exhibiting lamellar phase, namely, (a) parallel, (b) perpendicular, and (c) transverse alignment.

Flow alignment kinetics of the block copolymer with slightly different molecular weights has been studied thoroughly using rheo-optics.[5,9,17,22,23] By varying the temperature $T<T_{ODT}$, the shear strain amplitude γ_0 and the oscillation frequency ω, two distinct alignment directions of the lamellae can be obtained, namely, parallel and perpendicular (see Fig. 3). The third option, transverse alignment, is seldom observed because the equilibrium spacing is disturbed by shearing. The alignment, however, is hardly ever perfect and a combination of the alignments is often observed.

B. Rheological measurements

The samples were first pressed into small disks at 140 °C and subsequently cooled back to room temperature in order to obtain homogenous samples and to avoid unfavorable formation of air bubbles. After placing the samples between the quartz teeth they were heated above the order disorder transition temperature ($T_{ODT}\approx 170$ °C) up to 180 °C and kept there for 20 min in order to erase all history. Finally the samples were cooled down to the measurement temperature and were left to stabilize for 30 min. In the shearing experiments two different working temperatures were used, namely, 115 and 145 °C, whereas both the oscillation frequency ($\omega=1$ rad/s) and shear strain amplitude ($\gamma_0=0.42$) were kept constant.

Figure 4 shows the change of the dynamic storage (G') and loss moduli (G'') during the oscillatory shearing at

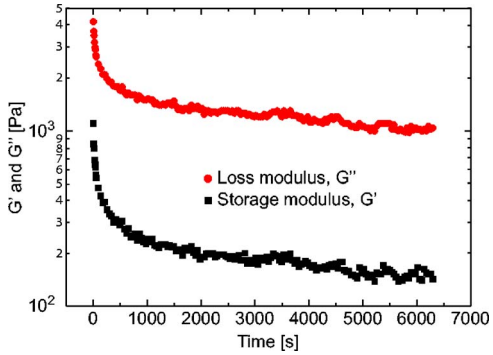

FIG. 4. (Color online) Evolution of the dynamic storage G' and loss modulus G'' of PS-*b*-PI during oscillatory shear at 115 °C. Oscillation frequency $\omega=1$ rad/s, shear strain amplitude $\gamma_0=0.42$.

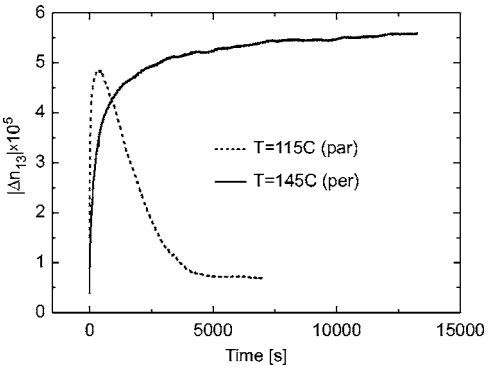

FIG. 5. Evolution of the birefringence during shear alignment at ($T=115$ °C) and ($T=145$ °C). Oscillation frequency $\omega=1$ rad/s, shear strain amplitude $\gamma_0=42\%$.

115 °C. Both moduli show a fast initial drop followed by a slow gradual decrease which is commonly observed for diblock copolymers undergoing shear-induced alignment.[9] The corresponding graph at 145 °C is not shown here because the torque response of the sample decreased to the limit of the sensitivity of the rheometer.

C. Flow birefringence measurements

As the laser beam propagates through the sample along the **−2**-direction (see Fig. 3) the projection of the refractive index tensor on the **1–3**-plane, i.e., $\Delta n_{13}=n_{11}-n_{33}$ is being measured. For lamellar PS-*b*-PI the form birefringence (Δn_f) is estimated to be at least three times the intrinsic birefringence (Δn_i) (Ref. 24) and thus the change in Δn_{13} can be directly related to changes in the block copolymer microstructure. For instance, the different alignment directions (see Fig. 3) of the lamellar diblock copolymer can now be identified from the Δn_{13} because, obviously, for parallel alignment $|\Delta n_{13}|\simeq 0$ whereas for perpendicular and transverse alignments $|\Delta n_{13}|>0$.

Dichroism and birefringence as well as their orientation angles were recorded before, during, and after rheological measurements. When the sample is subjected to LAOS conditions described in the previous section at 115 °C, birefringence shows a fast initial increase which is followed by a slow decay and flattening of the signal (see Fig. 5). Maintaining the shearing conditions and increasing the temperature to 145 °C leads to increased anisotropy as can be seen from the Fig. 5. Based on these results and earlier results obtained with a similar block copolymer[5] we may state that the former is progressing toward parallel and the latter toward perpendicular alignment. One should note the low level of the birefringence in the perpendicular case (the largest reported birefringence for a perpendicular alignment of PS-*b*-PI is[23] $\Delta n_{max}\simeq 1\times 10^{-3}$), which means that the alignment is only adequate and in addition the parallel alignment decays to nonzero value meaning that some of the domains are still aligned in the normal direction. However, more detailed characterization with, e.g., small-angle x-ray scattering is required to verify these conclusions.

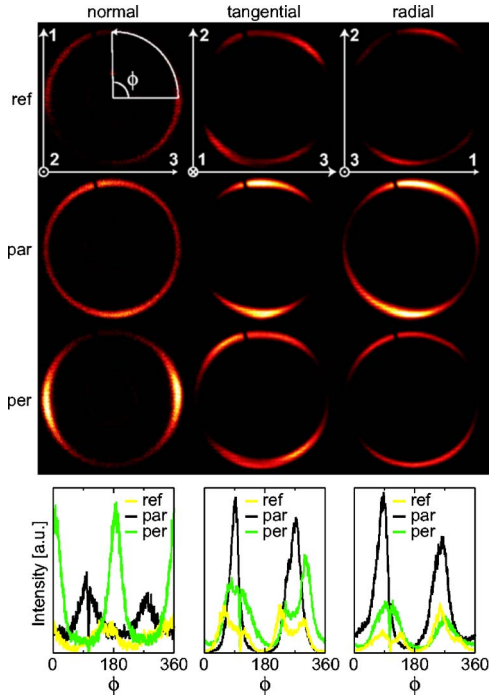

FIG. 6. (Color online) (Top) Two-dimensional SAXS patterns of the first order Debye ring in normal, tangential, and radial views for (ref) a reference sample and for samples subjected to LAOS (ω=1.0 rad/s, γ_0=42%) at 115 °C corresponding to parallel (par) alignment and at 145 °C corresponding to perpendicular (per) alignment. (Bottom) Azimuthal scans of the first order Debye rings along the curve illustrated in normal view of the reference sample.

D. Small-angle x-ray scattering measurements

After cessation of shear samples were cooled down to room temperature and removed carefully for an *ex situ* characterization. Samples were cut into small sections so that for each direction (normal, tangential, and radial) the path length of the x-ray beam was 1.0 mm.

X-ray scattering patterns were collected using a Bruker small-angle scattering system that includes a two-dimensional (2D) area detector (Bruker AXS). The generator was a Bruker Microstar rotating anode source with Montel Optics which was operated at 45 kV and 60 mA. The beam was further collimated using four sets of slits. The sample to detector distance was approximately 2500 mm. X-ray patterns were collected for 1000 s in normal, tangential, and radial views, i.e., with the incident beam along the **−2**, **−1**, and **−3** directions, respectively (see Fig. 3).

As a reference sample, we used an unaligned sample that has the same processing history as the aligned samples except it was not subjected to LAOS. The two-dimensional SAXS patterns of the samples are shown in Fig. 6 with the corresponding azimuthal scans at the bottom.

The scattering patterns verify the conclusions made in the previous section, i.e., at lower temperature (T=115 °C) the material processes toward parallel and at higher temperature (T=145 °C) toward perpendicular alignment. Neither of the alignments, however, is very good and particularly a combination of parallel and perpendicular alignment can be seen for the higher temperature case (see **per** in Fig. 6). This could already be interpreted from the optical signals but a combination of *in situ* birefringence measurements with *ex situ* structure characterization techniques is needed to give a thorough understanding of the shear aligned state especially when new materials are being studied.

ACKNOWLEDGMENTS

This work has been supported as part of the European Science Foundation Collaborative Research (EUROCORES) Programme on Self-Organized Nano-Structures (SONS). Dr. Janne Ruokolainen and Panu Hiekkataipale are acknowledged for the technical support during the SAXS experiments. The authors would also like to thank Sini Kivi and Klas Lindfors, Evgeny Polushkin, Charl Faul, and Gerrit ten Brinke for useful discussions.

[1] M. Muthukumar, C. K. Ober, and E. L. Thomas, Science **277**, 1225 (1997).
[2] F. S. Bates and G. H. Fredrickson, Phys. Today **52**, 32 (1999).
[3] I. W. Hamley, Angew. Chem., Int. Ed. **42**, 1692 (2003).
[4] O. Ikkala and G. ten Brinke, Chem. Commun. (Cambridge) **19**, 2131 (2004).
[5] Z. R. Chen, J. A. Kornfield, S. D. Smith, J. T. Grothaus, and M. M. Satkowski, Science **277**, 1248 (1997).
[6] J. Sänger, W. Gronski, H. Leist, and U. Wiesner, Macromolecules **30**, 7621 (1997).
[7] T. Thurn-Albrecht, J. Schotter, G. A. Kästle, N. Emley, T. Shibauchi, L. Krusin-Elbaum, K. Guarini, C. T. Black, M. T. Tuominen, and T. P. Russell, Science **290**, 2126 (2000).
[8] A. Böker, A. Knoll, H. Elbs, V. Abetz, A. H. E. Müller, and G. Krausch, Macromolecules **35**, 1319 (2002).
[9] V. K. Gupta, R. Krishnamoorti, J. A. Kornfield, and S. D. Smith, Macromolecules **28**, 4464 (1995).
[10] Y. M. Zhang and U. Wiesner, J. Chem. Phys. **106**, 2961 (1997).
[11] H. Leist, K. Geiger, and U. Wiesner, Macromolecules **32**, 1315 (1999).
[12] K. de Moel, R. Mäki-Ontto, M. Stamm, O. Ikkala, and G. ten Brinke, Macromolecules **34**, 2892 (2001).
[13] D. L. Polis, S. D. Smith, N. J. Terrill, A. J. Ryan, D. C. Morse, and K. I. Winey, Macromolecules **32**, 4668 (1999).
[14] E. Polushkin, G. A. van Ekenstein, O. Ikkala, and G. ten Brinke, Rheol. Acta **43**, 364 (2004).
[15] K. Mortensen, K. Almdal, F. S. Bates, K. Koppi, M. Tirrell, and B. Norden, Physica B **213**, 682 (1995).
[16] M. E. Vigild, C. Chu, M. Sugiyama, K. A. Chaffin, and F. S. Bates, Macromolecules **34**, 951 (2001).
[17] Z. R. Chen and J. A. Kornfield, Polymer **39**, 4679 (1998).
[18] R. M. Kannan and J. A. Kornfield, Macromolecules **27**, 1177 (1994).
[19] E. Polushkin, G. Alberda van Ekenstein, I. Dolbnya, W. Bras, O. Ikkala, and G. ten Brinke, Macromolecules **36**, 1421 (2003).
[20] S. J. Johnson, P. L. Frattini, and G. G. Fuller, J. Colloid Interface Sci. **104**, 441 (1985).
[21] G. G. Fuller, *Optical Rheometry of Complex Fluids* (Oxford University Press, New York, 1995).
[22] Z. R. Chen, A. M. Issaian, J. A. Kornfield, S. D. Smith, J. T. Grothaus, and M. M. Satkowski, Macromolecules **30**, 7096 (1997).
[23] V. K. Gupta, R. Krishnamoorti, Z. R. Chen, J. A. Kornfield, S. D. Smith, M. M. Satkowski, and J. T. Grothaus, Macromolecules **29**, 875 (1996).
[24] T. P. Lodge and G. H. Fredrickson, Macromolecules **25**, 5643 (1992).